

A New Single-Phase Switched-Coupled-Inductor DC–AC Inverter for Photovoltaic Systems

Kisu Kim, Honnyong Cha, *Member, IEEE*, and Heung-Geun Kim, *Senior Member, IEEE*

Abstract—This paper presents a new single-phase switched-coupled-inductor dc–ac inverter featuring higher voltage gain than the existing single-phase qZ-source and semi-Z-source inverters. Similar to the single-phase qZ-source and semi-Z-source inverters, the proposed inverter also has common grounds between the dc input and ac output voltages, which is beneficial especially for photovoltaic inverter systems. The inverter volume and maximum current flowing can be reduced significantly through the coupling of all inductors. A theoretical analysis of the proposed inverter is described and a 280-W experimental prototype is built to verify the performance of the inverter.

Index Terms—Common ground, dc–ac inverter, high voltage gain, qZ-source inverter, single-phase inverter, switched-coupled-inductor (SCL), Z-source inverter.

I. INTRODUCTION

NOWADAYS, there is an increasing demand for low-cost single-phase dc–ac inverters in many applications such as photovoltaic (PV), fuel cell, and battery powered systems. The conventional methods are shown in Fig. 1. Fig. 1(a) shows the well-known full-bridge (FB) inverter referred to as buck inverter in this paper [1]–[3]. In this circuit, the inverter output voltage (v_o) cannot be greater than input voltage (V_{in}). When the input voltage is low, a boost dc–dc converter is inserted between V_{in} and the inverter bridge as shown in Fig. 1(b). However, the two topologies in Fig. 1 have different input and output grounds. This may result in large leakage current in applications such as transformer-less grid-tied PV inverter, which will cause safety and electromagnetic interference problem [4]–[7].

In order to overcome the disadvantages of the conventional inverters, a large number of single-stage inverters are proposed [8], [9]. In addition, the Z-source inverter topologies overcome the limitations mentioned earlier [10]–[16].

Fig. 2(a) shows the current-fed (CF) single-phase qZ-source inverter [14], and Fig. 2(b) is the semi-qZ-source inverter [15],

Manuscript received April 26, 2016; revised July 5, 2016; accepted August 24, 2016. Date of publication September 7, 2016; date of current version February 27, 2017. This research was supported by the Basic Science Research Program through the National Research Foundation of Korea(NRF) funded by the Ministry of Science, ICT, and Future Planning (NRF-2013R1A2A2A01069038). Recommended for publication by Associate Editor H. Li.

K. Kim and H. Cha are with the School of Energy Engineering, Kyungpook National University, Daegu 1370, South Korea (e-mail: kimkisu1027@gmail.com; chahonny@knu.ac.kr).

H.-G. Kim is with the Department of Electrical Engineering, Kyungpook National University, Daegu 1370, South Korea (e-mail: hgkim@knu.ac.kr).

Color versions of one or more of the figures in this paper are available online at <http://ieeexplore.ieee.org>.

Digital Object Identifier 10.1109/TPEL.2016.2606489

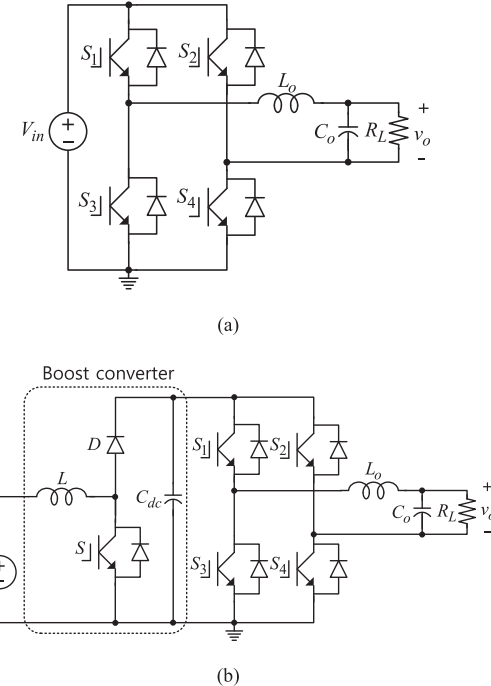


Fig. 1. Conventional single-phase inverters. (a) FB inverter. (b) FB inverter with dc–dc boost converter.

which is an improved version of Fig. 2(a). Both the inverters have the same voltage gain as shown below and require only two active switches to obtain the same maximum voltage gain as the FB inverter shown in Fig. 1(a)

$$\frac{v_o}{V_{in}} = \frac{2D - 1}{D}. \quad (1)$$

In (1), D is defined as the duty ratio of switch S_2 .

As shown in Fig. 2, the two topologies share common grounds between V_{in} and v_o , thus they can minimize the possible ground leakage current problem effectively [7] when they are used for PV inverter. However, as depicted in Fig. 2(c), their attainable maximum voltage gain is limited to 1, which means that they are not suitable for applications where input voltage is low.

In order to overcome the limitations of Fig. 2 while maintaining the doubly ground features, a three-switch three-state single-phase Z-source inverter (TSTS-ZSI) was introduced in [17]. Fig. 3 shows the boost-based TSTS-ZSI and buck-boost-based TSTS-ZSI, respectively. The inverters can have higher voltage gain than 1, and they comprise three switches, three capacitors, and three inductors.

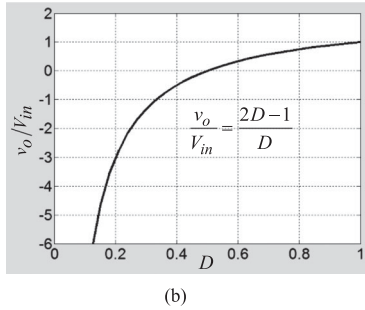
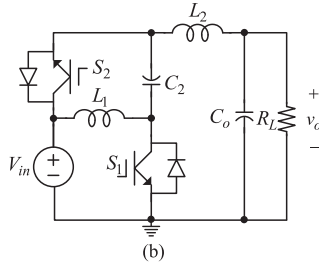
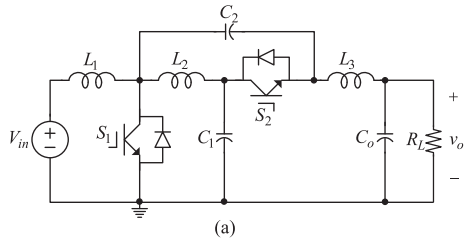


Fig. 2. Single-phase qZ-source inverters. (a) Single-phase CF-qZ-source inverter. (b) Semi-qZ-source inverter. (c) Voltage gain.

Although higher voltage gain is obtained, the three inductors (L_1 , L_2 , and L_3) in the TSTS-ZSI make the circuit a bit bulky and heavy. In addition, the switch signals of the inverter are all different and relatively complicated.

In this paper, a single-phase switched-coupled-inductor dc-ac inverter is proposed. Similar to the TSTS-ZSIs, the proposed inverter can obtain higher voltage gain than the circuits in Fig. 2 and maintains same ground between V_{in} and v_o . The proposed inverter also requires three active switches, but all the inductors in the circuit can be coupled together, which will lead to more compact and cost effective solution than the TSTS-ZSI. In addition, the switch signal generation is relatively simpler than the TSTS-ZSI. A 280-W prototype inverter is built and its performances are verified through experiment.

II. OPERATION PRINCIPLE OF THE PROPOSED DC-AC INVERTER

Fig. 4 shows the proposed inverter and it takes similar structure with the single-phase CF-qZ-inverter shown in Fig. 2(a). Compared with Fig. 2(a), the proposed inverter has an additional switch (S_x), capacitor (C_x), and inductor (L_2) coupled with inductor L_1 [18]–[19].

The inductors L_1 and L_2 are coupled with $1:n$ turns ratio and all the inductors in the proposed topology can be coupled altogether as will be discussed in Section III. The added $1:n$ coupled inductor contributes to the increase of voltage gain [16],

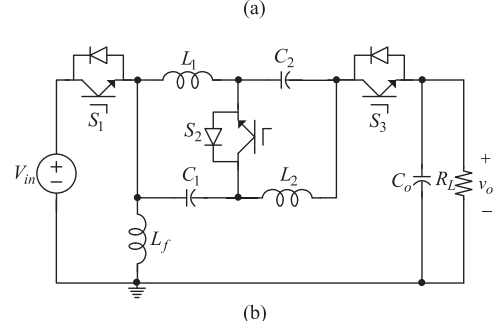
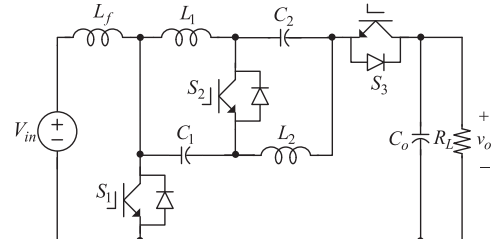


Fig. 3. Three-switch TSTS-ZSI [17]. (a) Boost-based TSTS-ZSI. (b) Buck-boost-based TSTS-ZSI.

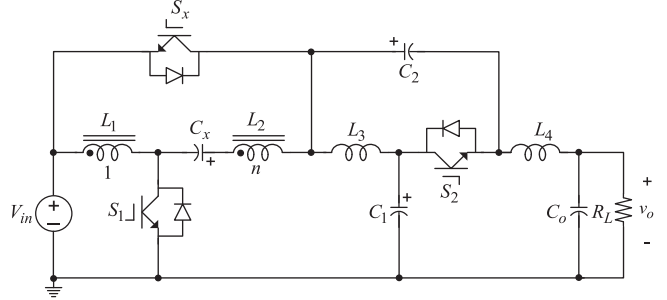


Fig. 4. Proposed dc-ac inverter.

[21]. Although the leakage inductance of the coupled inductor may induce a voltage spike across switch S_1 , this is not a major problem because such a voltage spike and the voltage of S_1 are low. In Section III, it will be found that the voltage stress of S_1 is always half of S_2 or S_x if leakage inductance is not considered. Therefore, as long as the voltage overshoot caused by the leakage inductance is not so high, the voltage stress of S_1 will be less than that of S_2 and there is not much problem in selecting switching device for S_1 . On the other hand, the leakage inductance is beneficial in limiting the current passing through C_x . Switches S_1 and S_2 are complementary as in the single-phase qZ-source inverter and the switch S_x is synchronized with S_1 .

A. Mode Analysis of the Proposed Inverter

Fig. 5 shows operation of the proposed inverter and there are two operational modes during one switching cycle. In mode 1, switches S_1 and S_x are turned-ON, and S_2 is turned-OFF. In mode 2, switches S_1 and S_x are turned-OFF, and S_2 is turned-ON. Followings are the detailed mode analysis of the proposed inverter.

In mode 1, the capacitor C_x is charged to $(n+1)V_{in}$. Since the C_x is being charged and discharged during one switching

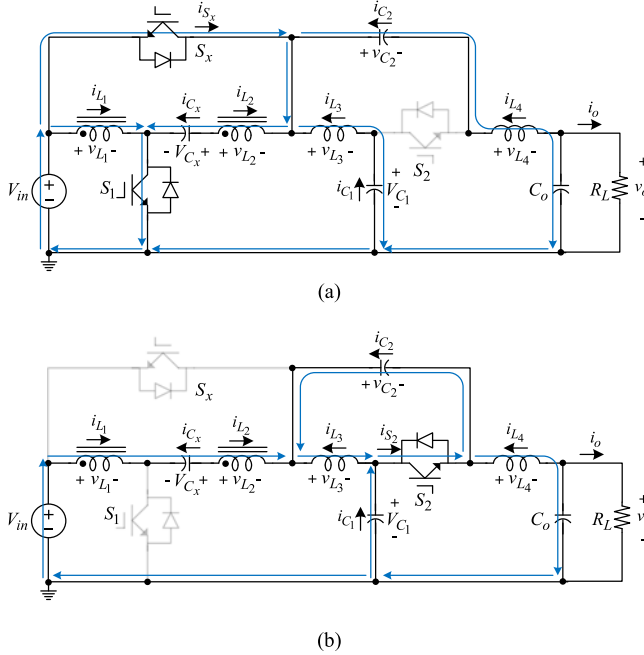


Fig. 5. Mode analysis of the proposed inverter. (a) Mode 1: \$S_1\$ and \$S_x\$ are ON, and \$S_2\$ is OFF. (b) Mode 2: \$S_1\$ and \$S_x\$ are OFF, and \$S_2\$ is ON.

period, its voltage has ripple and the ripple voltage depends on the output power [18]–[20]. Therefore, when the voltage difference between \$(n+1)V_{\text{in}}\$ and \$C_x\$ is high, relatively high surge (charging) current will flow through \$V_{\text{in}} - D_x(S_x) - L_2 - C_x - S_1\$ and the switching devices in this path (\$S_x\$ and \$S_1\$) can be damaged. In order to limit the high surge current, a current limiting inductor is necessary. In this paper, the leakage inductance generated by the coupling of \$L_1\$ and \$L_2\$ serves as the current limiting inductor. From Fig. 5(a), the voltage and current relations in mode 1 are derived as

$$V_{C_x} = V_{\text{in}} + v_{L_2} = (n+1)V_{\text{in}} \quad (2)$$

$$\begin{cases} v_{L_1} = V_{\text{in}} \\ v_{L_3} = V_{\text{in}} - V_{C_1} \\ v_{L_4} = V_{\text{in}} - v_{C_2} - v_o \end{cases} \quad (3)$$

$$\begin{cases} i_{C_1} = i_{L_3} \\ i_{C_2} = i_{L_4} \\ i_{C_x} = i_{\text{in}} - i_{L_1} + i_{L_3} + i_{L_4} \end{cases}. \quad (4)$$

In mode 2, capacitor \$C_x\$ is discharged by the inductor current, \$i_{L_1}\$. From Fig. 5(b), the voltage and current relations in mode 2 are derived as follows:

$$\begin{cases} (1+n)v_{L_1} = V_{\text{in}} + V_{C_x} - v_{C_2} - V_{C_1} \\ v_{L_3} = v_{C_2} \\ v_{L_4} = V_{C_1} - v_o \end{cases} \quad (5)$$

$$\begin{cases} i_{C_1} = -i_{L_1} - i_{L_4} \\ i_{C_2} = -i_{L_1} - i_{L_3} \\ i_{C_x} = -i_{L_1} \end{cases}. \quad (6)$$

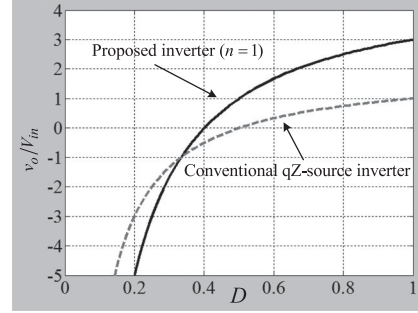


Fig. 6. Voltage gain comparison.

From the aforesaid equations, voltage relations are derived as follows:

$$V_{C_1} = v_{C_2} + v_o \quad (7)$$

$$V_{C_1} = (n+2)V_{\text{in}}. \quad (8)$$

From the flux (volt-second) balance condition on \$L_3\$, the capacitor \$C_2\$ voltage is derived as follows:

$$v_{C_2} = \frac{(1-D)(n+1)}{D} V_{\text{in}} \quad (9)$$

where \$D\$ is the duty cycle of switch \$S_2\$.

By using (7)–(9), the voltage gain of the proposed inverter is derived as follows:

$$\frac{v_o}{V_{\text{in}}} = \frac{(2n+3)(2D-1)+1}{2D} \leq n+2. \quad (10)$$

Fig. 6 shows the voltage gain of the proposed inverter when \$n=1\$ and compared with the conventional inverters shown in Fig. 2. It is found that the proposed inverter has a higher voltage gain than the conventional inverters shown in Figs. 1(a) and 2.

According to the charge balance condition on \$C_x\$, \$C_1\$, and \$C_2\$, the inductor currents averaged in one switching period are derived as follows:

$$i_{L_{1,\text{avg}}} = \frac{(2D-1)(n+1)}{D} i_o \quad (11)$$

$$i_{L_{2,\text{avg}}} = 0 \quad (12)$$

$$i_{L_{3,\text{avg}}} = i_{L_{4,\text{avg}}} = -i_o \quad (13)$$

$$i_{S_{2,\text{avg}}} = i_{S_{x,\text{avg}}} = i_o. \quad (14)$$

Currents of inductors \$L_1\$ and \$L_2\$ are different in respective mode unlike inductor currents \$i_{L_3}\$ and \$i_{L_4}\$. In mode 1, where current ripple is ignored, they are derived

$$i_{L_1} = \frac{(2D-1)(n+1-D)}{D(1-D)} i_o \quad (15)$$

$$i_{L_2} = -\frac{(2D-1)}{(1-D)} i_o. \quad (16)$$

In mode 2, they are expressed as follows:

$$i_{L_1} = i_{L_2} = \frac{2D-1}{D} i_o. \quad (17)$$

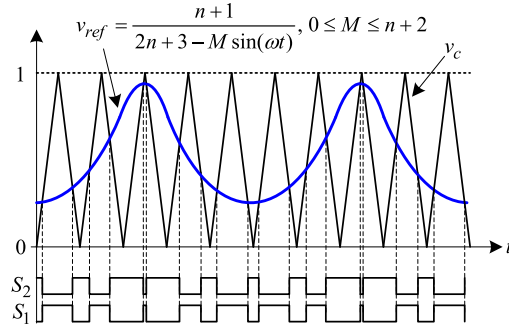


Fig. 7. Gate signal generation of the proposed inverter.

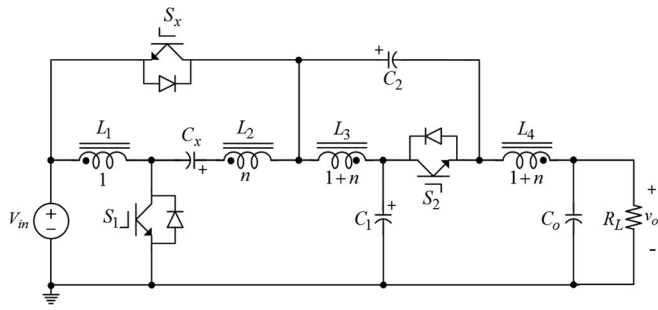


Fig. 8. Circuit topology of the proposed inverter when all inductors are coupled into one core.

B. Modulation Scheme of the Proposed Inverter

Modulation scheme of the proposed inverter is the same as that of the single-phase qZ-source inverter. By defining the output voltage of the inverter as (18), modulation index (M) of the inverter is derived as follows:

$$v_o = V_m \sin \omega t \quad (18)$$

$$M = \frac{V_m}{V_{in}}. \quad (19)$$

By substituting (18) and (19) into (10), the following duty cycle equation is derived as follows:

$$D = \frac{n + 1}{2n + 3 - M \sin(\omega t)}, \quad (0 \leq M \leq n + 2). \quad (20)$$

When $n = 1$ and $M = 3$, the duty cycle range of the proposed inverter is 0.25–1.0. Fig. 7 represents the gate signal generation of the proposed inverter. When reference signal (v_{ref}) is greater than the carrier signal (v_c), switch S_2 is turned on and switch S_1 is turned OFF.

III. MAGNETIC INTEGRATION OF INDUCTORS AND COMPARISON

A. Magnetic Integration of Inductors

As discussed in Section II, the L_1 and L_2 are coupled with $1:n$ ratio to obtain higher voltage gain. In this section, it is revealed that all the four inductors (L_1 , L_2 , L_3 , and L_4) in the proposed inverter can be coupled using one magnetic core.

TABLE I
DEVICE STRESS OF THE PROPOSED INVERTER

	Voltage stress	Current stress
S_1	$\frac{2n+3+M}{2M} V_o$	$\frac{(2n+3-M)(M-1)}{n+2-M} I_o$
S_2	$\frac{2n+3+M}{M} V_o$	$\frac{2n+3+M}{n+1} I_o$
S_x	$\frac{2n+3+M}{M} V_o$	$\frac{2n+3-M}{n+2-M} I_o$

The previous analysis shows that the voltages across each inductor during mode 1 are as follows:

$$\begin{cases} v_{L_1} = V_{in} \\ v_{L_2} = nV_{in} \\ v_{L_3} = V_{in} - V_{C_1} = -(n+1)V_{in} \\ v_{L_4} = V_{in} - v_{C_2} - v_o = -(n+1)V_{in} \end{cases}. \quad (21)$$

Similarly, the voltages across each inductor during mode 2 are as follows:

$$\begin{cases} v_{L_1} = \frac{1}{n+1}(V_{in} + V_{C_x} - V_{C_1} - v_{C_2}) = -\frac{1}{n+1}v_{C_2} \\ v_{L_2} = -\frac{n}{n+1}v_{C_2} \\ v_{L_3} = v_{C_2} \\ v_{L_4} = V_{C_1} - v_o = v_{C_2} \end{cases}. \quad (22)$$

From (21) and (22), it is found that regardless of the operating mode, the four inductors in the proposed inverter have the following voltage relationships:

$$v_{L_1} : v_{L_2} : v_{L_3} : v_{L_4} = 1 : n : -(n+1) : -(n+1). \quad (23)$$

Therefore, all the inductors can be coupled using one core [22], which leads to significant reduction in magnetic volume and converter size. It should be noted that n is the turns ratio and it is not the real number of turns. Fig. 8 shows the final completed circuit of the proposed inverter with the inductor polarity dots marked. The operation with magnetic integration is the same as that of the previous analysis in Section II.

B. Comparison of Switch Stress and Others

From Fig. 5 and (8), (9), (21), (22), voltage stresses of the three switches can be determined. Similarly, the switch current stresses can be determined from (4), (6), (13)–(17) and Fig. 5. Table I shows maximum switch stress of the proposed inverter. Table II compares the proposed inverter when $n = 1$ with the boost based TSTS-ZSI shown in Fig. 3(a). k is maximum of modulation index [17].

Although the buck-boost-based TSTS-ZSI has lower device stresses, it has drawbacks like more complicated gate signal generation, discontinuous input and output current, and requires additional LC filter that builds the circuit structure more complex and large inductor [17]. For these reasons, the boost-based TSTS-ZSI is compared with the proposed inverter.

From the result of Table II, it is evident that the overall voltage and current stresses of the proposed inverter are greater than

TABLE II
COMPARISON OF INVERTERS

		Proposed inverter ($n = 1$)		Boost based TSTS-ZSI ($k = 3$)	
		Voltage stress	Current stress	Voltage stress	Current stress
S_1		$\frac{5+M}{2M}V_o$	$\frac{(M-1)(5-M)}{3-M}I_o$		
S_2			$\frac{5+M}{2}I_o$	$\frac{5}{M}V_o$	$(M+2)I_o$
S_x		$\frac{5+M}{M}V_o$	$\frac{5-M}{3-M}I_o$		
No. of capacitors		4		3	
No. of inductors		1 (coupled inductor)		3 (discrete inductors)	
Current	Input	Quasi-continuous		Continuous	
	Output	Continuous		Discontinuous	
Gate signal generation		Relatively simple		Complex	
$\Delta i_{L_{\max}}$		$\Delta i_{L_1} = \Delta i_{L_2} = \frac{(3+M)(1+M)}{(5+M)^2} \times \frac{V_{in}T_s}{L_1}$, $\Delta i_{L_3} = \Delta i_{L_4} = \frac{4(3+M)}{(5+M)^2} \times \frac{V_{in}T_s}{L_3}$ ($L_1 = L_2, L_3 = L_4$)		$\Delta i_{L_f} = \frac{4}{5} \times \frac{V_{in}T_s}{L_f}, \Delta i_{L_1} = \Delta i_{L_2} = \frac{5}{4} \times \frac{V_{in}T_s}{L_{1,2}}$ ($L_1 = L_2$)	
$i_{L_{avg}}$ (one switching period)		$i_{L_1_avg} = I_o(M \sin(\omega t) - 1),$ $i_{L_2_avg} = 0, i_{L_3_avg} = i_{L_4_avg} = -I_o \sin \omega t$		$i_{L_f_avg} = I_o M \sin \omega t,$ $i_{L_1_avg} = i_{L_2_avg} = I_o \sin \omega t$	
$V_{C_{\max}}$		$V_{C_x} = \frac{2}{M}V_o, V_{C_1} = \frac{3}{M}V_o, V_{C_2} = \frac{3+M}{M}V_o$		$V_{C_1} = V_{C_2} = \frac{5+M}{2M}V_o$	

those of the TSTS-ZSI and the proposed inverter requires one more capacitor. However, current stress of the proposed inverter is lower than that of the boost-based TSTS-ZSI when M is lower than 2.4. Moreover, the proposed inverter can reduce the magnetic volume through the coupling of all separate inductors. Comparison of maximum current ripple, average current, and maximum capacitor voltage is summarized in Table II. According to the Table II, when compared with the boost-based TSTS-ZSI, the inductor current ripples of the proposed inverter are reduced by more than 2 due to coupling effect. In Table II, L_1 and L_3 of the proposed inverter are self-inductances of the coupled inductor. In addition, self-inductances L_1 and L_2 of the proposed inverter are the same and L_3 and L_4 are also the same when all inductors are coupled with $n = 1$. The boost-based TSTS-ZSI is assumed that L_1 and L_2 are equal [17]. Although, the C_2 capacitor voltage of the proposed inverter is greater than that of the boost-based TSTS-ZSI, the capacitor voltages of C_x and C_1 in the proposed converter are lower than those of the boost-based TSTS-ZSI. Moreover, inductor has more influence on size and weight than capacitor. The average inductor currents of the proposed inverter and boost-based TSTS-ZSI in one switching period are almost the same.

In conclusion, the proposed inverter can reduce overall magnetic volume because lower inductance is required. In addition, the boost-based TSTS-ZSI should have large output capacitor

TABLE III
ELECTRICAL SPECIFICATIONS OF THE PROPOSED INVERTER

Output power	280 W
Input voltage	62 Vdc
Output voltage	110 Vrms / 60 Hz
Switching frequency	20 kHz
IGBT (S_x, S_1, S_2)	FGH40N60
Coupled inductor	Core EE7066
	Inductance (L_1, L_2) 60 uH
	Inductance (L_3, L_4) 240 uH
Capacitance (C_x, C_1)	100 uF
Capacitance (C_o)	4.4 uF

because of discontinuous output current. Moreover, the gate signal generation of the proposed inverter is much simpler than that of the TSTS-ZSI.

IV. EXPERIMENTAL RESULTS

A 280-W prototype inverter is built and tested. Detailed electrical specifications of the proposed inverter are summarized in Table III.

As already mentioned in Section II, a relatively small current limiting inductor is required in the path $V_{in} - D_x(S_x) - L_2 - C_x - S_1$ to limit the high surge current. In the proposed circuit, the leakage inductance (about 300 nH) generated by

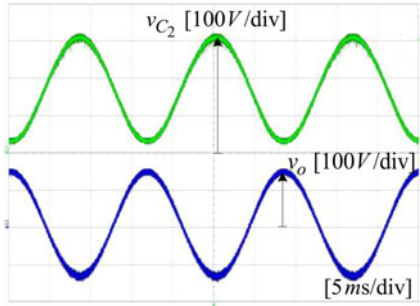


Fig. 9. Experimental waveforms of the proposed inverter. (v_{C_2} , v_o)

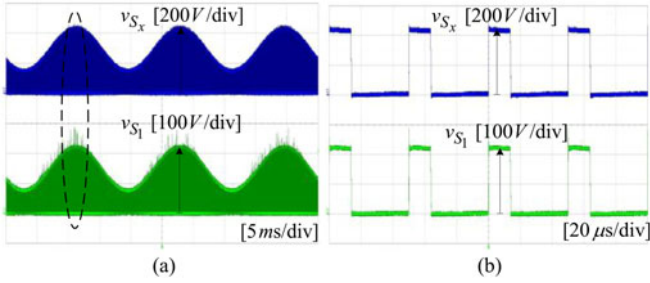


Fig. 10. Experimental waveforms of the proposed inverter (v_{S_x} , v_{S_1}). (a) Switching waveform. (b) Zoomed-in waveform of (a).

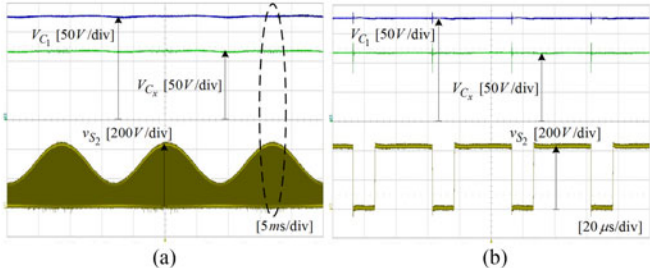


Fig. 11. Experimental waveforms of the proposed inverter (v_{S_2} , V_{C_1} , V_{C_x}). (a) Switching waveform. (b) Zoomed-in waveform of (a).

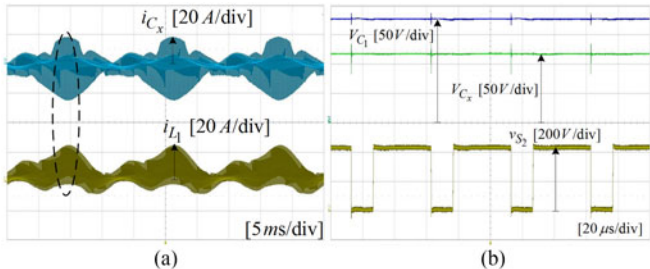


Fig. 12. Experimental waveforms of the proposed inverter. (a) Current waveforms (i_{L_1} , i_{C_x}). (b) Zoomed-in waveform of (a).

coupling of L_1 and L_2 is used for this purpose. Followings are the experimental waveforms of the proposed inverter when $V_{in} = 62$ V, $M = 2.5$, and $P_o = 280$ W.

Fig. 9 shows the experimental waveform of the output voltage and the capacitor C_2 voltage. Figs. 10 and 11 show the voltages across all switches (v_{S_x} , v_{S_1} , and v_{S_2}). As expected, there is

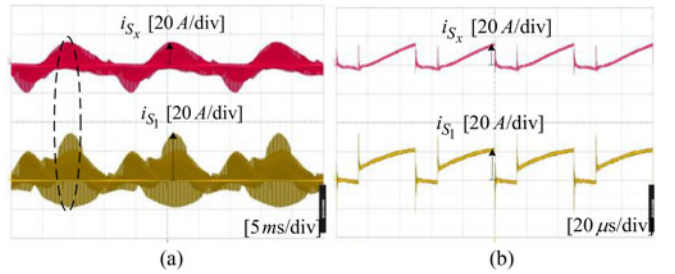


Fig. 13. Experimental waveforms of the proposed inverter. (a) Switch current waveforms (i_{S_x} , i_{S_2}). (b) Zoomed-in waveform of (a).

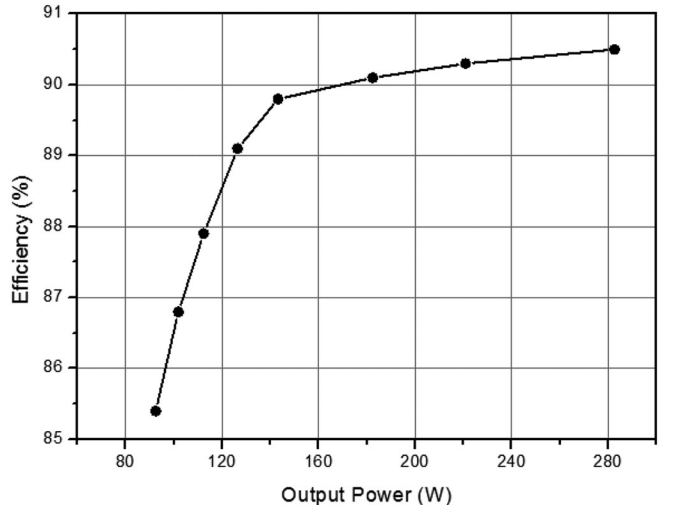


Fig. 14. Efficiency of the proposed inverter.

voltage overshoot in switch S_1 caused by the leakage inductance and there are no noticeable overshoots in the switches S_2 voltage varying with D , the voltages across C_1 and C_x are almost constant and they are fixed to $3V_{in}$ and $2V_{in}$, respectively. Figs. 12 and 13 show current waveforms. shows the efficiency of the proposed inverter tested with $V_{in} = 62$ V with output power varies.

V. CONCLUSION

In this paper, the single-phase switched coupled inductor dc-ac inverter was presented. It has an operation principle similar to that of a single-phase qZ-source inverter. With the addition of components S_x , C_x , and the coupled inductor, voltage gain of the proposed inverter can be extended to greater than 2. The magnetic integration of all inductors decreases the converter volume significantly and the proposed inverter has relatively simple gate signal generation. Moreover, similar to the single-phase qZ-source inverter and the TSTS-ZSI, the proposed inverter shares common grounds between the dc input and the ac output voltage. A 280-W prototype inverter was built and tested to verify operation of the proposed inverter.

REFERENCES

- [1] T. Kawabata, K. Honjo, N. Sashida, K. Sanada, and M. Koyama, "High-frequency link dc/ac converter with PWM cycloconverter," in Proc. IEEE IAS Conf., 1990, pp. 1119–1124.

- [2] N. R. Zargari, P. D. Ziogas, and G. Joos, "A two-switch high-performance current regulated dc/ac converter module," *IEEE Trans. Ind. Appl.*, vol. 31, no. 3, pp. 583–589, May./Jun. 1995.
- [3] M. D. Bellar, T.-S. Wu, A. Tchamdjou, J. Mahdavi, and M. Ehsani, "A review of soft-switched dc-ac converters," *IEEE Trans. Ind. Appl.*, vol. 34, no. 4pp. 847–860, Jul./Aug. 1998.
- [4] J. M. A. Myrzik and M. Calais, "String and module integrated inverters for single-phase grid connected photovoltaic systems: A review," in *Proc. IEEE Bologna Power Tech Conf.*, 2003, vol. 2, pp. 430–437.
- [5] O. Lopez *et al.*, "Eliminating ground current in a transformerless photovoltaic application," *IEEE Trans. Energy Convers.*, vol. 25, no. 1, pp. 140–147, Mar. 2010.
- [6] S. Araujo, P. Zacharias, and R. Mallwitz, "Highly efficient single-phase transformerless inverters for grid-connected photovoltaic systems," *IEEE Trans. Ind. Electron.*, vol. 57, no. 9, pp. 3118–3128, Sep. 2010.
- [7] N. Vazquez, M. Rosas, C. Hernandez, E. Vazquez, and F. J. Rerez-Rinal, "A new common-mode transformerless photovoltaic inverter," *IEEE Trans. Ind. Electron.*, vol. 62, no. 10, pp. 6381–6391, Oct. 2015.
- [8] Q. Li and P. Wolfs, "A review of the single phase photovoltaic module integrated converter topologies with three different DC link configurations," *IEEE Trans. Power Electron.*, vol. 23, no. 3, pp. 1320–1333, May 2008.
- [9] Y. Xue, L. Chang, S. B. Kjær, J. Bordonau, and T. Shimizu, "Topologies of single-phase inverters for small distributed power generators: An overview," *IEEE Trans. Power Electron.*, vol. 19, no. 5, pp. 1305–1314, Sep. 2004.
- [10] F. Z. Peng, "Z-source inverter," *IEEE Trans. Ind. Appl.*, vol. 39, no. 2, pp. 504–510, Mar./Apr. 2003.
- [11] J. Anderson and F. Z. Peng, "Four quasi-Z-Source inverters," in *Proc. IEEE Power Electron. Specialists Conf.*, 2008, pp. 2743–2749.
- [12] S. Yang, F. Z. Peng, Q. Lei, R. Inoshita, and Z. Qian, "Current-fed quasi-z-source inverter with voltage buck-boost and regeneration capability," *IEEE Trans. Ind. Appl.*, vol. 47, no. 2, pp. 882–892, Mar./Apr. 2011.
- [13] W. Qian, F. Z. Peng, and H. Cha, "Trans-Z-source inverters," *IEEE Trans. Power Electron.*, vol. 26, no. 12, pp. 3453–3463, Dec. 2011.
- [14] Y. Tang, S. Xie, and C. Zhang, "Single-phase Z-Source inverter," *IEEE Trans. Power Electron.*, vol. 26, no. 12, pp. 3869–3873, Dec. 2011.
- [15] D. Cao, S. Jiang, X. Yu, and F. Z. Peng, "Low-cost semi-Z-source inverter for single-phase photovoltaic systems," *IEEE Trans. Power Electron.*, vol. 26, no. 12, pp. 3514–3523, Dec. 2011.
- [16] F. Ahmed, H. Cha, S. Kim, and H. Kim, "Switched-coupled-inductor quasi-Z-source inverter," *IEEE Trans. Power Electron.*, vol. 31, no. 2, pp. 1241–1254, Feb. 2016.
- [17] L. Huang, M. Zhang, L. Hang, W. Yao, and Z. Lu, "A Family of three-switch three-state single-phase Z-source inverters," *IEEE Trans. Power Electron.*, vol. 28, no. 5, pp. 2317–2329, May 2013.
- [18] F. L. Luo and H. Ye, "Positive output super-lift converters," *IEEE Trans. Power Electron.*, vol. 18, no. 1, pp. 105–113, Jan. 2003.
- [19] F. L. Luo and H. Ye, "Positive output multiple-lift push-pull switched-capacitor Luo-converters," *IEEE Trans. Ind. Electron.*, vol. 51, no. 3, pp. 594–602, Jun. 2004.
- [20] M. Shen, F. Z. Peng, and L. M. Tolbert, "Multilevel DC-DC power conversion system with multiple DC sources," *IEEE Trans. Power Electron.*, vol. 23, no. 1, pp. 420–426, Jan. 2008.
- [21] M. Rico, J. Uceda, J. Sebastian, and F. Aldana, "Static and dynamics modeling of tapped-inductor DC-to-DC converters," *Proc. IEEE Power Electron. Specialists Conf.*, 1987, pp. 281–288.
- [22] A. F. Witulski, "Introduction to modeling of transformers and coupled inductors," *IEEE Trans. Power Electron.*, vol. 10, no. 3, pp. 349–357, May 1995.



Kisoo Kim received the B.S. degree in electrical engineering from Kyungpook National University, Daegu, South Korea, in 2015. He is currently working toward the M.S. degree in the School of Energy Engineering, Kyungpook National University.

His current research interests include magnetic design, buck and boost inverters, and three-phase transformer design.



Honnyong Cha (S'08–M'10) received the B.S. and M.S. degrees in electronics engineering from Kyungpook National University, Daegu, South Korea, in 1999 and 2001, respectively, and the Ph.D. degree in electrical engineering from Michigan State University, East Lansing, MI, USA, in 2009.

From 2001 to 2003, he was a Research Engineer in the Power System Technology (PSTEK) Company, Ansan, South Korea. From 2010 to 2011, he was a Senior Researcher at the Korea Electrotechnology Research Institute, Changwon, South Korea. In 2011, he joined as an Assistant Professor in the School of Energy Engineering, Kyungpook National University. His current research interests include high-power dc–dc converters, dc–ac inverters, Z-source inverters, and power conversion for electric vehicles and wind power generation.



Heung-Geun Kim (S'82–M'88–SM'12) was born in South Korea in 1956. He received the B.S., M.S., and Ph.D. degrees in electrical engineering from Seoul National University, Seoul, South Korea, in 1980, 1982, and 1988, respectively.

Since 1984, he has been with the Department of Electrical Engineering, Kyungpook National University, Daegu, South Korea, where he is currently a Full Professor and the Director in the Microgrid Research Center. He was a Visiting Scholar in the Department of Electrical and Computer Engineering, University of Wisconsin-Madison, Madison, WI, USA, from 1990 to 1991, and at the Department of Electrical Engineering, the Michigan State University, Lansing, MI, USA, from 2006 to 2007. His current research interests include ac machine control, PV power generation, and microgrid system.